CHEMISTRY OF MATERIALS

ARTICLE

pubs.acs.org/cm

Topochemical Synthesis of Sodium Metal Phosphate Olivines for Sodium-Ion Batteries

Kyu Tae Lee,[†] T. N. Ramesh,[†] F. Nan,[‡] G. Botton,[‡] and Linda F. Nazar*[,†]

[†]University of Waterloo, Department of Chemistry, 200 University Avenue West, Waterloo, Ontario, Canada N2L 3G1

[‡]McMaster University, Department of Material Science and Engineering, Hamilton, Ontario, Canada L8S 4L7

Supporting Information

ABSTRACT: New metastable olivine phases of sodium metal phosphates, $Na[Mn_{1-x}M_x]PO_4$ (M = Fe, Ca, Mg), nanorods are synthesized by a simple solid-state reaction at low temperature (≤100 °C) by means of a topotactic molten salt reaction that converts $NH_4[Mn_{1-x}M_x]PO_4•H_2O$ (M = Fe, Ca, Mg) to $Na[Mn_{1-x}M_x]PO_4$. Their crystal structures are characterized via XRD Rietveld refinement and electron diffraction. A full range of solid solution behavior was observed for olivine $Na_{1-x}Mn_{0.5}Fe_{0.5}PO_4$, in contrast to that of $LiMPO_4$ (M = Fe, Mn) olivine materials, and is ascribed to ion size effects. The solid solution behavior of $NaMn_{0.5}Fe_{0.5}PO_4$ was confirmed by electrochemical characterization.

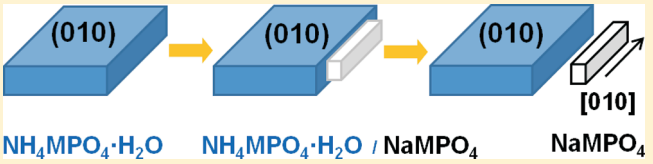

KEYWORDS: olivine, Na-ion battery, topotactic, low-temperature synthesis, cathode material

INTRODUCTION

Lithium-ion batteries play a vital role as the prominent power sources for cell phones, laptop computers, digital cameras, power tools, electrical assist bicycles, and many consumer products. They are now also attracting tremendous interest as energy storage devices for automotive applications. In upcoming years, many electric vehicles and extended range electric vehicles will be powered by large-scale lithium-ion storage batteries. At the present time, lithium resources are confirmed to be unevenly distributed, located primarily in South America. The cost of lithium-based raw materials has roughly doubled from the first practical application in 1991 to now, and it may drastically increase when the demand for lithium increases as a result of commercialization of large-scale lithium-ion batteries in the future. However, sodium resources are inexhaustible and unlimited everywhere around the world. Furthermore, the electrochemical equivalent and standard potential of sodium are the most advantageous for aprotic battery applications after lithium. However, only a limited number of successful reports are found concerning sodium insertion electrode materials. Regarding oxide-based positive electrodes, Doeff et al.[1] and Braconier et al.[2,3] reported the reversible de(intercalation) of Na from $Na_{0.44}MnO_2$ and Na_xMO_2 (M = Co, Cr, Ni), respectively, at high potential, and the Bruce group[4] has recently reported the same for $Na_{0.44}MnO_2$ using a sodium polymer electrolyte. Tarascon et al. demonstrated it is possible to (de)intercalate Na ions in λ-MnO_2[5] and $Na_xMo_2O_4$.[6] Regarding low potential materials capable of Na-insertion necessary for the negative electrode, Doeff et al.[7] and Dahn[8] demonstrated that Na ions can be electrochemically de/inserted in hard carbons; and recently, Alcantara et al.[9] and Komaba et al.[10] introduced the concept of using metal oxide materials. In the case of phosphate-based cathodes, similarly, only a handful of materials have been developed, namely, $NaVPO_4F$[11] (reported to have a tavorite structure), $Na_3V_2(PO_4)_3F_3$,[12] and Na_2FePO_4F.[13−15] The latter has numerous advantages over the first, including a layered structure that is particularly suitable for ion mobility and an inexpensive nontoxic metal. However, it suffers a little from the viewpoint of gravimetric capacity and energy density owing to the 3.4 V redox couple. Direct formation of a sodium metal phosphate with an olivine structure would be very desirable, especially for a low-cost nontoxic metal such as iron or especially manganese, which has a higher voltage redox couple and hence a theoretically higher energy density. Mixed $Li[Fe,Mn]PO_4$ olivines have been shown to be especially promising. However, both $NaFePO_4$ and $NaMnPO_4$ form as an electrochemically inactive maricite phase under conventional synthetic conditions at high temperature, not the olivine phase.[16] Very recently, olivine-type $NaFePO_4$ has been electrochemically accessed using a positive electrode containing a mixture of 70% $FePO_4$ obtained by delithiation of olivine $LiFePO_4$, and 30% carbon.[17] Here, we introduce new metastable mixed metal olivine-type phases of $Na[Mn_{1-x}M_x]PO_4$ (M = Fe, Ca, Mg), where $0 \le x \le 0.5$, directly synthesized by a low-temperature solid-state method using a topatactic reaction and report their unusual solid solution behavior.

EXPERIMENTAL SECTION

Synthesis of $Na[Mn_{1-x}M_x]PO_4$. Ammonium metal phosphates $NH_4MPO_4•H_2O$ (M = Mn, $Mn_{0.5}Fe_{0.5}$, $Mn_{0.8}Ca_{0.2}$, $Mn_{0.8}Mg_{0.2}$) were synthesized according to previously reported methods[18−21] with modification. The materials were ground together with excess sodium acetate

Received: February 13, 2011
Revised: June 26, 2011
Published: July 20, 2011

trihydrate ($CH_3CO_2Na•3H_2O$), and heated between 65−100 °C to form $Na[Mn_{1-x}M_x]PO_4$ (M = Fe, Ca, Mg), where $0 \le x \le 0.5$. Unreacted sodium acetate trihydrate was removed by washing with ethanol. The oxidation of $NaMPO_4$ ($M = Fe_{0.5}Mn_{0.5}$) was accomplished using a slight excess of $NOBF_4$ or NO_2BF_4 in acetonitrile to obtain $Na_{0.5}MPO_4$ and $Na_{0.2}MPO_4$, respectively.

Synthesis of $NaFePO_4$. $LiFePO_4$ was oxidized with a slight excess of $NOBF_4$ in acetonitrile for 5 h to obtain $FePO_4$, which was reduced with excess NaI in acetonitrile for two days to obtain Na_xFePO_4 ($0 < x \le 1$).

Materials Characterization. Powder X-ray diffraction (XRD) data was collected on a Bruker D8-Advance powder diffractometer using Cu Kα radiation (λ = 1.5405 Å) operating from 2θ = 10−80°. Lattice parameters were determined using full pattern matching on the basis of an initial olivine-type *Pnma* unit cell in the GSAS platform employing the EXPGUI interface, followed by Rietveld refinement. Scale factor, zero point, lattice parameters, atomic positions, and atomic displacement parameters were iteratively refined. For refinement of the $NaMPO_4$ cells (M = Mn and $M = Fe_{0.5}Mn_{0.5}$), antisite mixing on the M1 and M2 sites was permitted, with the constraint that the total occupation on either of the M1 and M2 sites was equal to one. For $M = Fe_{0.5}Mn_{0.5}$, the Fe^{2+} and Mn^{2+} occupancy was additionally constrained to be equal on the basis of the ICP results that indicated the ratio of the two metals was the predicted 1:1 because XRD cannot distinguish between the scattering from Fe and Mn. Refinement of $Na[Mn_{0.8}Mg_{0.2}]PO_4$ also permitted antisite mixing on the M1 and M2 sites, with the constraint that the total occupation on either of the M1 and M2 sites was equal to one. The occupation on the M1 site included both Na^+ and Mn^{2+}, but Mg^{2+} occupation was not refined owing to the lack of distinction between scattering from Na^+ and Mg^{2+}. In this case, the Mn^{2+} occupancy on the M1 site defines the degree of antisite mixing; a reasonable assumption because the total Mn^{2+} occupancy on both M1 and M2 sites independently refined to 0.807 (close to the expected value of 0.8). Similarly, only Mn^{2+} and Mg^{2+} were refined on the M2 site (not Na^+), with a total occupation on that site constrained to be one. Refinement of the XRD pattern $Na_{0.5}[Mn_{0.5}Fe_{0.5}]PO_4$ was complicated by X-ray line broadening. Therefore, the occupancies of the Mn and Fe were fixed at 0.5, and only the Na occupancy was refined.

The SEM samples were examined in a LEO 1530 field-emission scanning electron microscope (FE-SEM) instrument equipped with an energy dispersive X-ray spectroscopy (EDX) attachment. TEM investigations were performed using a Philips CM12 operated at 120 kV or a JEOL-2010F electron microscope at an accelerating voltage of 200 kV with a field-emission gun (FEG).

Electrochemistry. Samples of electrochemically active materials were mechanically mixed for 1 h with carbon black and polyvinylidene fluoride in a 60:20:20 weight ratio. The electrochemical performance was evaluated using 2220 coin cells, using a Na metal anode, and 1 M $NaClO_4$ in a propylene carbonate electrolyte solution. Room temperature galvanostatic experiments were performed at a current density of 3.87 mA/g (C/40).

■ RESULTS AND DISCUSSION

Synthesis of $Na[Mn_{1-x}M_x]PO_4$. The thermodynamically stable form of $NaFePO_4$ is the mineral maricite. It is similar to the well-known $LiFePO_4$ olivine structure in terms of its phosphate framework, but the M1 and M2 sites are occupied by Fe^{2+} and Na^+, respectively, which is exactly the reverse of $LiFePO_4$ (Figure 1). This gives rise to a different connectivity of the Fe and Na octahedra, which blocks Na-ion migration pathways and, hence, results in a structure that is not amenable to Na^+ (de)insertion. $NaMnPO_4$ adopts the maricite structure in its thermodynamically stable form and has also been reported as the mineral natrophilite,

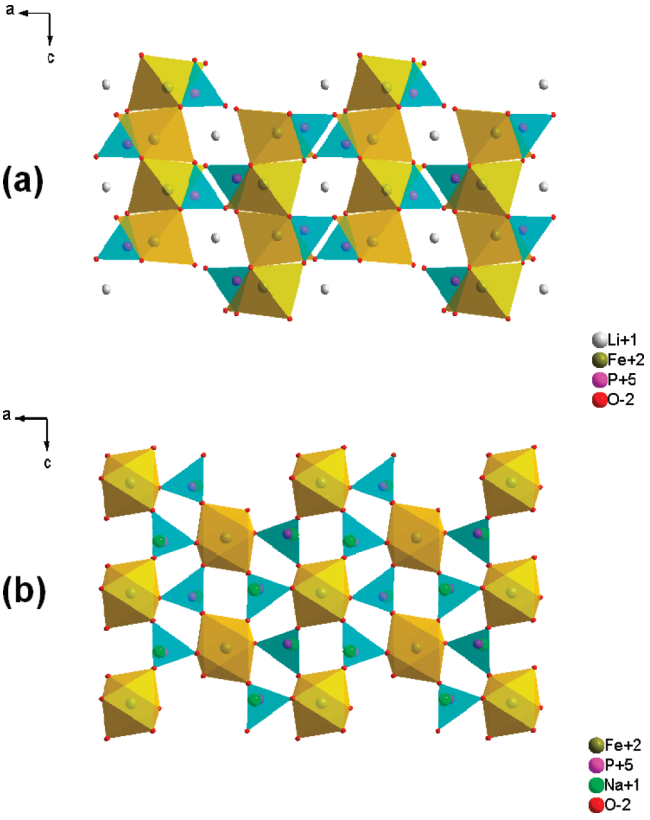

Figure 1. Structures of (a) olivine and (b) maricite shown in the 101 plane.

where the M1 and M2 sites are both half occupied by Mn^{2+} and Na^+. It is similarly electrochemically inactive.

The crystallization of $Na[Fe,Mn]PO_4$ as a metastable olivine phase thus entails the use of low-temperature synthesis methods. Our approach is to employ a low-temperature molten salt synthesis on the basis of our previous work detailing the topotactic transformation of $NH_4FePO_4•H_2O$ to $LiFePO_4$ in hydrothermal media,[22] which was also recently adopted for the synthesis of $LiMnPO_4$ using $NH_4MnPO_4•H_2O$ as a precursor.[23] We reasoned that the transformation of $NH_4MPO_4•H_2O$ to $NaMPO_4$ could follow a topotactic pathway by direct ion exchange between NH_4^+ and Na^+ using molten $CH_3CO_2Na•3H_2O$. As anticipated, the reaction of ammonium metal phosphates $NH_4MPO_4•H_2O$ (M = Mn, $Mn_{0.5}Fe_{0.5}$, $Mn_{0.8}Ca_{0.2}$, $Mn_{0.8}Mg_{0.2}$) with sodium acetate trihydrate ($CH_3CO_2Na•3H_2O$) between 65−100 °C readily formed the desired olivine $Na[Mn_{1-x}M_x]PO_4$ (M = Fe, Ca, Mg) phases, where $0 \le x \le 0.5$. The Ca^{2+}- or Mg^{2+}-substituted $NaMnPO_4$ olivine phases were prepared with ∼20% substitution of the alkaline earth ion targeted on the Mn^{2+} site, in order to allow for the possibility of adjusting the framework slightly to favor Na^+ mobility. However, the olivine phase of the pure iron compound $NaFePO_4$ could not be prepared by this direct method. Maricite was produced instead because $NH_4FePO_4•H_2O$ decomposes about 100 degrees lower than the temperature at which ion exchange occurs.[21] The $NaFePO_4$ olivine phase was prepared by a chimie douce method as described earlier:[24] olivine $LiFePO_4$ was delithiated at room temperature with $NOBF_4$ to form the orthorhombic phase of $FePO_4$, which was then sodiated with excess NaI.

dx.doi.org/10.1021/cm200450y |*Chem. Mater.* 2011, 23, 3593–3600

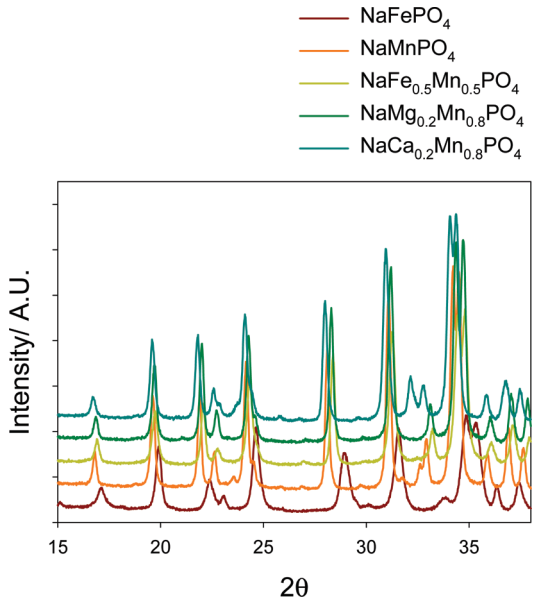

Figure 2. XRD patterns of $NaMPO_4$ (M = $Mn_{0.5}Fe_{0.5}$, Mn, Fe, $Mn_{0.8}Ca_{0.2}$, $Mn_{0.8}Mg_{0.2}$).

The corresponding X-ray diffraction (XRD) patterns of the materials shown in Figure 2 are in good accord with the predicted patterns on the basis of crystallization of the target olivine phases. Rietveld refinement of the XRD patterns was carried out for the selected materials, $NaMnPO_4$, $NaFePO_4$, $Na[Mg_{0.2}Mn_{0.8}]PO_4$, and $NaFe_{0.5}Mn_{0.5}PO_4$, to confirm their structures (Figure 3). The Ca-substituted phase, $Na[Ca_{0.2}Mn_{0.8}]PO_4$, was not readily amenable to Rietveld methods owing to its lower crystallinity, and therefore, its XRD pattern was indexed using CRYSFIRE. The lattice parameters are summarized in Table. 1. Those of $NaFePO_4$ synthesized by chemical insertion of Na are in good agreement with a $NaFePO_4$ phase that was just recently reported, derived by employing $FePO_4$ as a cathode in a Na-ion battery.[17] No evidence for any antisite mixing (exchange of Na^+/Fe^{2+} on their respective M1 and M2 sites) was found when this was an allowed parameter freed in the refinement.

The new mixed metal phases prepared by molten salt synthesis have lattice parameters between their end members, showing they are solid solution phases with respect to metal occupation on the M2 site. The unit cell volume of $NaFe_{0.5}Mn_{0.5}PO_4$ lies halfway between that of $NaFePO_4$ and $NaMnPO_4$, for example. Similarly, Mg^{2+} substitution on the Mn^{2+} site decreases the unit cell volume in accord with its smaller cation size (72 pm compared to 83 pm, whereas Ca^{2+} substitution on the M2 site results in an increase as expected from its cationic dimensions (100 pm compared to 83 pm). EDX analysis also confirmed that the targeted levels of Mg and Ca substitution in the lattice were achieved (vide infra). Larger values for the *b* and *c* axes and cell volume for $NaMnPO_4$ (V = 334 Å^3) and $Na[Fe_{0.5}Mn_{0.5}]PO_4$ (V = 329 Å^3) compared to their lithium congeners (V = 302.2 Å^3 and 296.1 Å^3 for $LiMnPO_4$ and $Li[Fe_{0.5}Mn_{0.5}]PO_4$, respectively[25]) reflect the larger size of Na (102 pm) compared to that of lithium (76 pm). Importantly, the occupancies of both M1 and M2 sites were allowed to vary during the final stages of the refinements to allow for antisite mixing, and we found that these materials have little cation disorder on the order of 2−3% (Table 1 and Supporting Information). The antisite disorder was

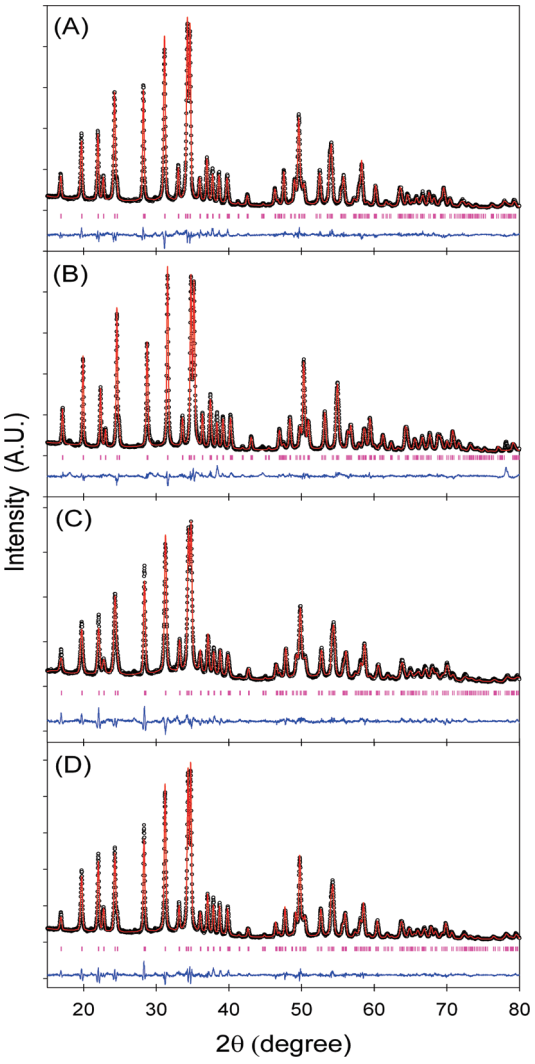

Figure 3. Rietveld refinements of $NaMPO_4$ for M as indicated: (a) Mn, (b) Fe, (c) $Fe_{0.5}Mn_{0.5}$, and (d) $Mg_{0.2}Mn_{0.8}$. Experimental points are in black. The fit is shown in red. Calculated reflections are in magenta. The difference map is shown in blue.

negligible in $Na[Mn_{0.8}Mg_{0.2}]PO_4$ on the basis of the refined occupancy (0.004) of Mn^{2+} on the M1 site (although the corresponding refinement of Na^+ on the M2 site was thwarted by the similarity in scattering between Na^+ and Mg^{2+}).

The overall low degree of cation disorder is an advantage of the proposed topatactic reaction sequence, which is illustrated in Figure 4. Comparison of the structures of olivine $NaMPO_4$ and $NH_4MPO_4•H_2O$ (M = Fe, Mn, Mg) indicates how they could be related by a simple transformation. The connectivity of the iron and phosphate polyhedra in the (100) plane of $NaMPO_4$ in the *Pnma* space group is identical to that in the corresponding (101) plane of $NH_4MPO_4•H_2O$ in the $Pmn2_1$ space group; note the difference in their space groups simply switches the *a* and *b* axes. Thus, repeating polyhedral motif is the same in the two cases as shown in Figure 4. Upon ion exchange of NH_4^+ for Na^+, the adjacent sheets are knitted together by condensation of the NaO_6 octahedra to crystallize the olivine $NaMPO_4$. The structure of the $NH_4MPO_4•H_2O$ precursors is perfectly ordered because of the bulky NH_4 ions, and thus, this order is faithfully replicated in the structure of the resulting products. The temperature is too low to

dx.doi.org/10.1021/cm200450y |*Chem. Mater.* 2011, 23, 3593–3600

Table 1. Lattice Parameters of $Na_{1-x}MPO_4$ (M = Fe, Mn, $Fe_{0.5}Mn_{0.5}$, $Mg_{0.2}Mn_{0.8}$, $Ca_{0.2}Mn_{0.8}$) Compounds Obtained from Rietveld Refinement

olivine	*a* (Å)	*b* (Å)	*c* (Å)	volume (Å^3)	R_p (%)	R_{wp} (%)	R_F^2 (%)	antisite mixing (%)
$NaFePO_4$	10.4207(5)	6.2167(2)	4.9529(2)	320.86(3)	4.91	7.42	9.08	–
$NaMnPO_4$	10.5578(3)	6.3359(2)	4.9966(2)	334.24(2)	5.32	6.99	5.62	1.9
$NaFe_{0.5}Mn_{0.5}PO_4$	10.4933(3)	6.2960(2)	4.9803(2)	329.03(3)	5.07	6.83	3.59	0.5
$Na_{0.5}Fe_{0.5}Mn_{0.5}PO_4$	10.2675(5)	6.0905(2)	4.9610(3)	310.24(2)	5.90	6.22	9.02	–
$NaMg_{0.2}Mn_{0.8}PO_4$	10.5158(3)	6.3083(1)	4.9841(1)	330.63(2)	6.00	7.60	5.03	0.9
$NaCa_{0.2}Mn_{0.8}PO_4$[a]	10.62	6.38	5.02	340		–		

[a] Cell parameters indexed using CRYSFIRE.

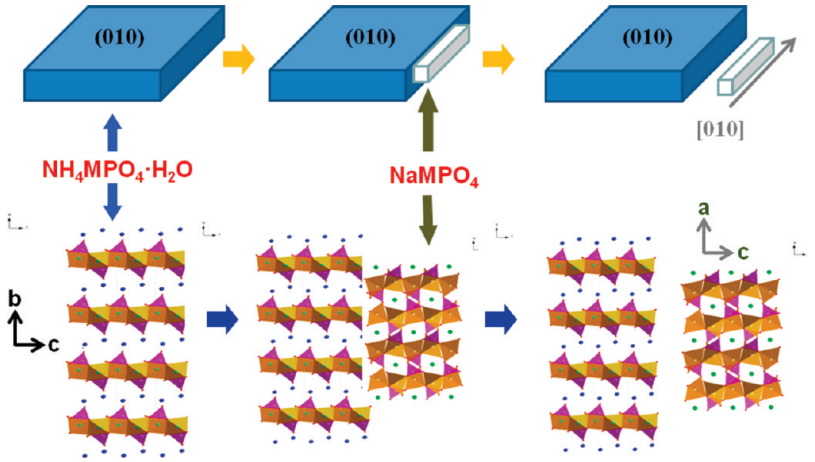

Figure 4. Schematic diagram for the topochemical synthesis of crystalline $NaMPO_4$ nanorods.

induce significant atomic position rearrangements such as switching of the M^{2+}/Na^+ ions.

SEM images (Figure 5) reveal the transformation of the flat plate morphology of the layered $NH_4MPO_4•H_2O$ crystals to the nanorod morphology of the $NaMPO_4$ olivine structure. The formation of nanorods is caused by a high interface strain at the grain boundaries between $NH_4MPO_4•H_2O$ and $NaMPO_4$. The *d*-spacing corresponding to the (010) reflection in $NH_4MPO_4•H_2O$ is quite different from the equivalent (100) reflection for $NaMPO_4$ owing to the size of the bulk NH_4^+ ion in the interlayer space; for example, in the case of M = Mn, d_{010} = 8.8 Å ($NH_4MnPO_4•H_2O$) and d_{100} = 4.7 Å ($NaMnPO_4$). Although the replacement of NH_4^+ for Na^+ is topotactic, it is not instantaneous within the interlayer gallery, and hence, this large mismatch induces cleavage during the ion exchange process that creates nanorods (Figure 4). On the basis of the topatactic transformation of $NH_4MPO_4•H_2O$ to $NaMPO_4$ (vide supra), the long axis of the $NaMPO_4$ nanorod must be either the *b* or *c* axis. Our TEM and electron diffraction studies (Figure 6a) reveal that the long axis of all the $NaMPO_4$ nanorods is the *b* axis, which is the facile direction of ion transport for olivine materials. However, the nanorod morphology can be altered by ball-milling the material, ideally with carbon, to enhance the conductivity of the material for use as a sodium-ion electrode. Elemental analysis carried out in the TEM using EDS confirmed that Mg and Ca were substituted into their respective $Na[Mg_{0.2}Mn_{0.8}]PO_4$, and $Na[Ca_{0.2}Mn_{0.8}]PO_4$ lattices (Figure 6b,c) in the targeted levels (see Figures 1S and 2S of the Supporting Information for expanded versions of the EDS spectra).

Of significance is that although $NaFePO_4$ cannot be prepared directly by the molten salt method, this is easily accomplished for all of the $NaMnPO_4$ compounds (including substitution with 1/2 Fe and/or Mg). The olivine phase does convert to the more stable maricite phases at about 450 °C for $NaFePO_4$ at a higher temperature, about 500 °C for $Na[Fe_{0.5}Mn_{0.5}]PO_4$, and at the highest temperature, about 550 °C for $NaMnPO_4$, as shown by XRD patterns (Figure 7). Thus, the olivine $NaMPO_4$ materials are metastable phases but are perfectly stable under normal operating conditions of an electrochemical cell containing a nonaqueous electrolyte.

Solid-State Chemistry of $Na[Mn_{1-x}M_x]PO_4$. Desodiation of olivine $Na(Fe_{0.5}Mn_{0.5})PO_4$ to form $Na_{0.5}(Fe_{0.5}Mn_{0.5})PO_4$ and $Na_{0.2}(Fe_{0.5}Mn_{0.5})PO_4$ surprisingly forms a single-phase composition as shown by XRD (Figure 8). The XRD peaks gradually shift to higher 2θ angles as the degree of Na extraction increases, and no evidence for a two-phase mixture of the end member phases is observed. The amount of desodiation was independently measured by EDS analysis (Figure 3S of the Supporting Information), confirming the expected decrease in Na content with increasing *x* in $Na_{1-x}(Fe_{0.5}Mn_{0.5})PO_4$. Formation of the single phase of $Na_{0.5}(Fe_{0.5}Mn_{0.5})PO_4$ was confirmed by Rietveld refinement and gave good agreement factors as shown in Figure 9. The occupancy of Na was refined to be 0.509, very close to the target value. The $Na_{0.5}(Fe_{0.5}Mn_{0.5})PO_4$ phase was stable under air at room temperature for more than at least two months, as shown by XRD (Figure 10).

The above is in strong contrast to the distinct two-phase behavior on delithiation observed for $LiFePO_4$ but similar to that

dx.doi.org/10.1021/cm200450y |*Chem. Mater.* 2011, 23, 3593–3600

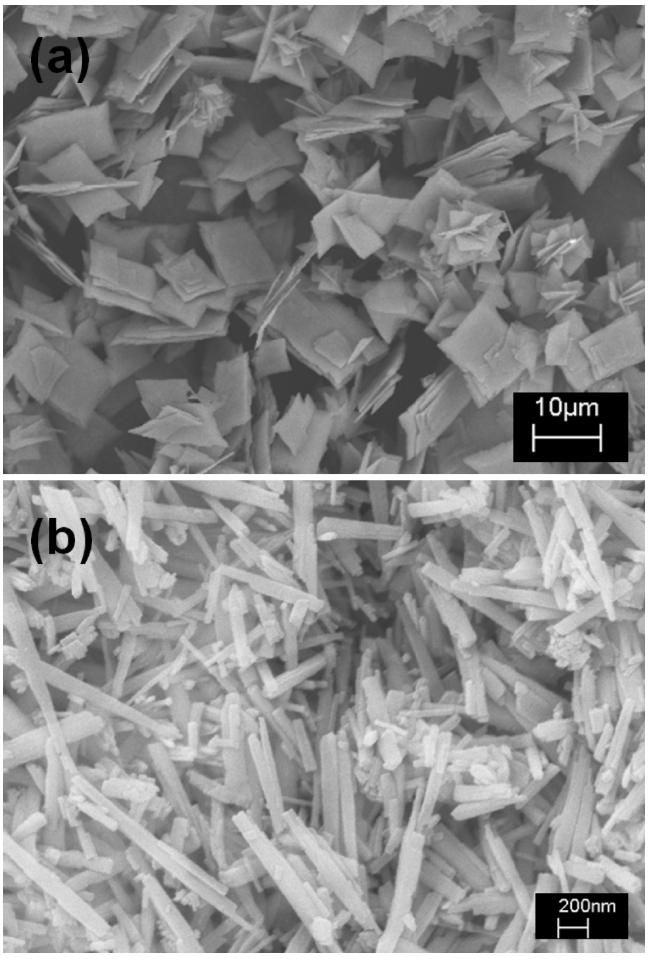

Figure 5. SEM images of (a) $NH_4MPO_4 \cdot H_2O$ and (b) $NaMPO_4$.

observed for delithiation of $Li(Fe_xMn_y)PO_4$ (i.e, $x = 0.6$, $y = 0.4$) to form $Li_{0.5}(Fe_xMn_y)PO_4$ originally reported by Yamada et al.[26] This has been studied theoretically by Ceder et al.,[27] and experimentally confirmed by Molenda et al.[28] for a composition very close to $Li_{0.5}(Fe_{0.5}Mn_{0.5})PO_4$. However, the latter shows limited solid solution behavior, but $Na(Fe_{0.5}Mn_{0.5})PO_4$ exhibits solid solution behavior over the full region. The volume difference between two phases is a critical factor to determine whether a solid solution is formed. On the basis of the Hume−Rothery rules for metals, the formation of a solid solution is unfavorable when the atomic radii of the solute and solvent atoms differ by more than 15%. In case of $Na(Fe_{0.5}Mn_{0.5})PO_4$, the volume difference is 21%, which is much larger than the corresponding volume difference for $LiFePO_4$ (6.7%). Therefore, this phenomenon is not explained by the previous simple model. It seems that the driving force to make the solid solution is the interface stress caused by significant strain at the grain boundaries between Na-rich and Na-poor phases of $Na_{1-x}(Fe_{0.5}Mn_{0.5})PO_4$. The interface effect on the formation of solid solutions in intercalation compounds has been suggested by Wagemaker et al.[29] They showed the miscibility gap decreases as the size of Li_xTiO_2 nanoparticles decreases. It can be attributed to the energy penalty due to interface energy:

$$\Delta G_{mix}(X) = \frac{(x_2 - x)G_1 - (x - x_1)G_2}{x_2 - x_1} - \Delta G(X) + \frac{A(x)\gamma}{v_{Li}V}$$

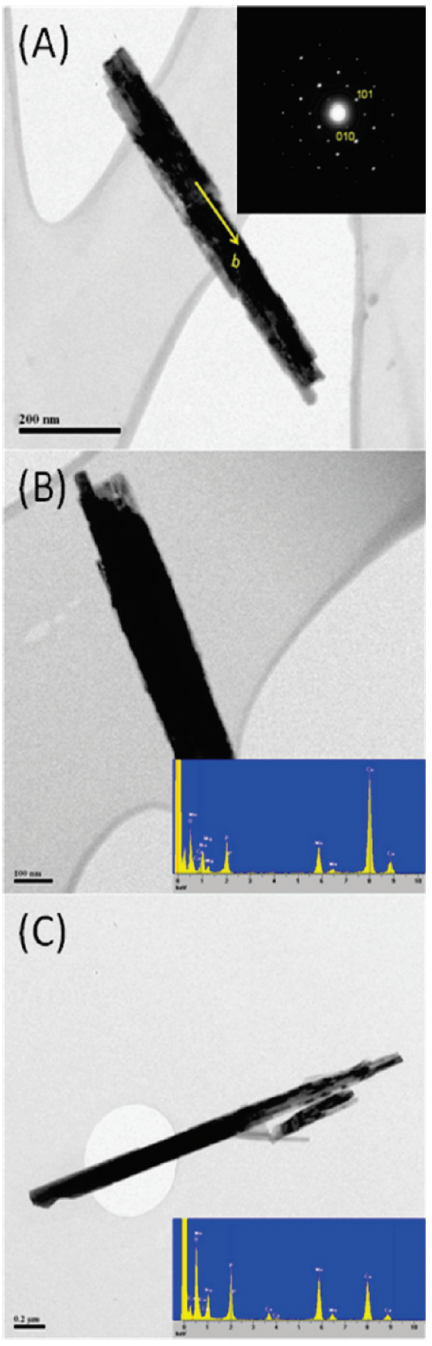

Figure 6. TEM images of (a) $NaMnPO_4$ (inset: SAED pattern), (b) $NaMg_{0.2}Mn0.8PO_4$ (inset: EDS profile), and (c) $NaCa_{0.2}Mn0.8PO_4$ (inset: EDS profile).

where $A(x)$, γ, v_{Li}, V are the area of the interface between the two phases 1 and 2, the interface energy, the (inserted) Li-ion molar volume, and the volume of the particle, respectively. The last term is related to the interface energy, and its effect becomes more dominant as particle size decreases, because $A(x)$ and V scale with r^2 and r^3, respectively (where r is the particle radius). Therefore, the energy gain due to phase separation, represented by the free energy of mixing ΔG_{mix} decreases for smaller particle sizes, resulting in the decrease in miscibility gap for Li_xTiO_2 nanoparticles. In the case of $Na(Fe_{0.5}Mn_{0.5})PO_4$, the particle size is small. Conversely,

dx.doi.org/10.1021/cm200450y |*Chem. Mater.* 2011, 23, 3593–3600

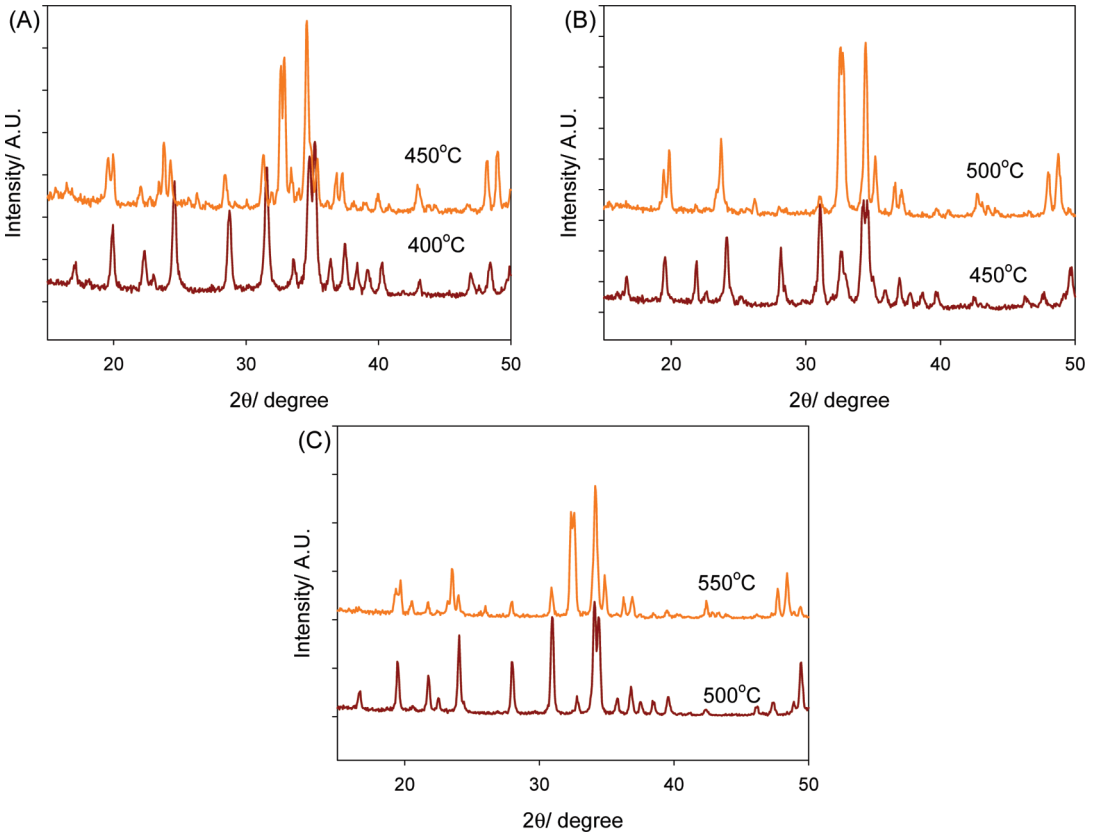

Figure 7. Olivine-to-maricite transition temperatures of $NaMPO_4$. XRD patterns of $NaMPO_4$ for M as indicated: (a) Fe, (b) $Mn_{0.5}Fe_{0.5}$, and (c) Mn) at various temperatures.

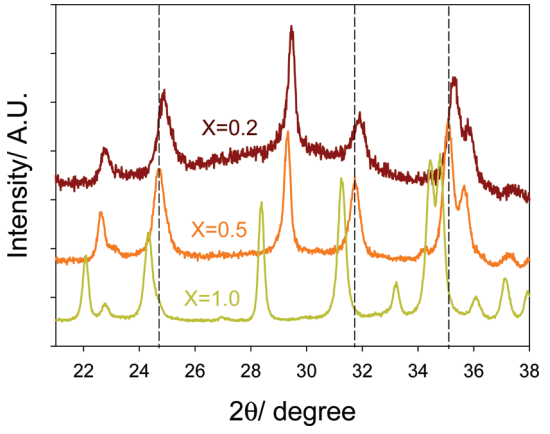

Figure 8. XRD patterns of $Na_xFe_{0.5}Mn_{0.5}PO_4$ for varying degrees of x.

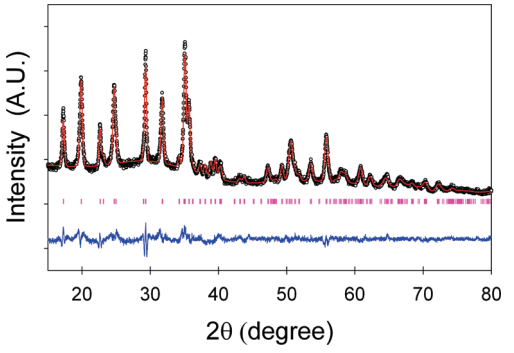

Figure 9. Rietveld refinement of $Na_{0.5}Fe_{0.5}Mn_{0.5}PO_4$. Experimental points are in black. The fit is shown in red. Calculated reflections are in magenta. The difference map is shown in blue.

the interface energy, γ, is very high due to the high interface strain owing to the large size of the Na ion. Therefore, a single-phase regime is formed. The electrochemical data is in complete accord with a single-phase reaction (Figure 11), although kinetic limitations may induce a sloping voltage profile. This is currently under investigation in our laboratory.

Finally, as $FePO_4$ is partially sodiated, the XRD reflections for $Na_{1-x}FePO_4$ are noticeably shifted compared to $NaFePO_4$ but not continuously. We observe formation of a single phase on partial desodiation of $NaFePO_4$ to $Na_{1-x}FePO_4$ ($x \sim 0.4$) (Figure 12), although the substantial peak broadening, and appearance of a second phase ($FePO_4$) precluded Rietveld refinement of the structure. The new phase has very similar lattice parameters to that of recently reported $Na_{0.7}FePO_4$, whose refinement suggests is a very interesting single line phase.[17] Our finding that it forms in equilibrium with the $FePO_4$ end member at intermediate values of x fully supports that conclusion. Its formation may be attributed to subtle factors that drive interface strain between $NaFePO_4$ and $FePO_4$ and force cation ordering, forces that are clearly different than those that dictate single-phase formation in $Na_{1-x}Mn_{0.5}Fe_{0.5}PO_4$.

dx.doi.org/10.1021/cm200450y |*Chem. Mater.* 2011, 23, 3593–3600

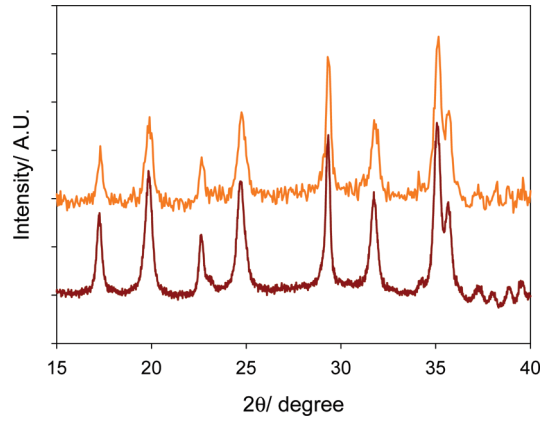

Figure 10. Phase stability of $Na_{0.5}Fe_{0.5}Mn_{0.5}PO_4$. XRD patterns of $Na_{0.5}Fe_{0.5}Mn_{0.5}PO_4$: (a) as prepared (brown profile) and (b) after two months (orange profile).

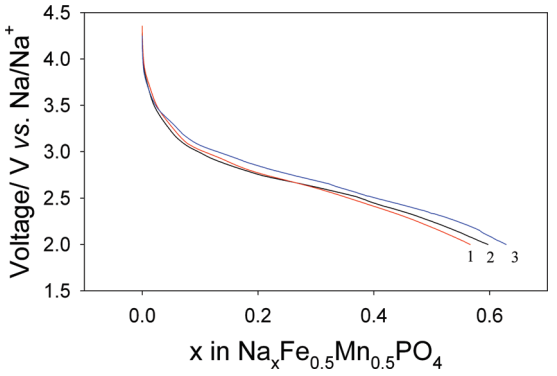

Figure 11. Discharge profile of $NaMn_{0.5}Fe_{0.5}PO_4$ over three cycles as labeled.

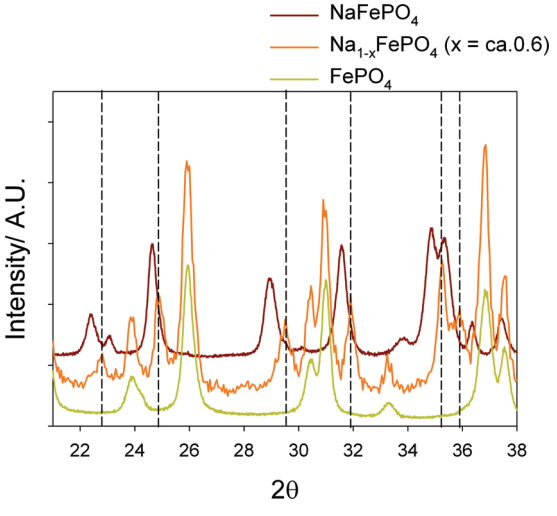

Figure 12. XRD patterns of $Na_{1-x}FePO_4$, formed by desodiation of $NaFePO_4$. Dotted lines indicate the reflections due to the new phase which has similar parameters to those of $Na_{0.7}FePO_4$;[17] other reflections are due to the second component of the mixture, $FePO_4$.

CONCLUSIONS

In summary, metastable olivine phases of crystalline Na-$[Mn_{1-x}M_x]PO_4$ (M = Fe, Ca, Mg) are formed by topatactic reactions using simple solid-state synthesis in molten salts at low (≤100 °C) temperatures. This is in contrast to the high-temperature synthesis of $NaMnPO_4$, for example, which forms the electrochemically inactive maricite phase. $Na(Fe_{0.5}Mn_{0.5})PO_4$ exhibits a single-phase reaction on desodiation, not a two-phase reaction as in the case of $LiFePO_4$. Both nanorod formation and the solid solution behavior of $Na[Mn_{1-x}M_x]PO_4$ are closely related to the large interface strain between the Na-rich and Na-poor phases due to the large size of the Na ion. $Na[Mn_{1-x}M_x]PO_4$ exhibited reversible electrochemical de/intercalation, making these materials potentially interesting as cathode materials in sodium ion batteries. The detailed electrochemistry of the carbon-coated materials in the $NaMPO_4$ (M = Mn, Fe, Mg, Ca) family will be reported in a forthcoming publication with in situ and ex situ XRD analysis.

ASSOCIATED CONTENT

Supporting Information. EDS profile of $Na[Mg_{0.2}Mn_{0.8}]PO_4$, $Na[Ca_{0.2}Mn_{0.8}]PO_4$, and $Na_xFe^{0.5}Mn_{0.5}PO_4$; CIF files in tabular form; lattice constants and atomic parameters of $NaFePO_4$, $NaMnPO_4$, $Na[Mn_{0.5}Fe_{0.5}]PO_4$, $Na_{0.5}[Fe_{0.5}Mn_{0.5}]PO_4$, and $Na[Mg_{0.2}Mn_{0.8}]PO_4$ refined from powder XRD data. This material is available free of charge via the Internet at http://pubs.acs.org.

AUTHOR INFORMATION

Corresponding Author
*E-mail: lfnazar@uwaterloo.ca.

ACKNOWLEDGMENT

NSERC is gratefully acknowledged for financial support. We thank B. Ellis and S. Oh for helpful discussions.

REFERENCES

(1) Doeff, M. M.; Peng, M. Y.; Ma, Y. P.; Dejonghe, L. C. *J. Electrochem. Soc.* **1994**, *141*, L145.
(2) Braconnier, J. J.; Delmas, C.; Fouassier, C.; Hagenmuller, P. *Mater. Res. Bull.* **1980**, *15*, 1797.
(3) Braconnier, J. J.; Delmas, C.; Hagenmuller, P. *Mater. Res. Bull.* **1982**, *17*, 993.
(4) Zhang, C. H.; Gamble, S.; Ainsworth, D.; Slawin, A. M. Z.; Andreev, Y. G.; Bruce, P. G. *Nat. Mater.* **2009**, *8*, 580.
(5) Tarascon, J. M.; Guyomard, D. G.; Wilkens, B.; McKinnon, W. R.; Barboux, P. *Solid State Ionics* **1992**, *57*, 113.
(6) Tarascon, J. M.; Hull, G. W. *Solid State Ionics* **1986**, *22*, 85.
(7) Doeff, M. M.; Ma, Y. P.; Visco, S. J.; Dejonghe, L. C. *J. Electrochem. Soc.* **1993**, *140*, L169.
(8) Stevens, D. A.; Dahn, J. R. *J. Electrochem. Soc.* **2001**, *148*, A803.
(9) Alcantara, R.; Jaraba, M.; Lavela, P.; Tirado, J. L. *Chem. Mater.* **2002**, *14*, 2847.
(10) Komaba, S.; Mikumo, T.; Yabuuchi, N.; Ogata, A.; Yoshida, H.; Yamada, Y. *J. Electrochem. Soc.* **2010**, *157*, A60.
(11) Barker, J.; Saidi, M. Y.; Swoyer, J. L. *Electrochem. Solid State Lett.* **2003**, *6*, A1.
(12) Gover, R. K. B.; Bryan, A.; Burns, P.; Barker, J. *Solid State Ionics* **2006**, *177*, 1495.
(13) Ellis, B. L.; Makahnouk, W. R. M.; Rowan-Weetaluktuk, W. N.; Ryan, D. H.; Nazar, L. F. *Chem. Mater.* **2010**, *22*, 1059.
(14) Recham, N.; Chotard, J. N.; Dupont, L.; Djellab, K.; Armand, M.; Tarascon, J. M. *J. Electrochem. Soc.* **2009**, *156*, A993.

(15) Ellis, B. L.; Makahnouk, W. R. M.; Makimura, Y.; Toghill, K.; Nazar, L. F. *Nat. Mater.* **2007**, *6*, 749.
(16) Bridson, J. N.; Quinlan, S. E.; Tremaine, P. R. *Chem. Mater.* **1998**, *10*, 763. Moring, J.; Kostiner, E. *J. Solid State Chem.* **1986**, *61*, 379.
(17) Moreau, P.; Guyomard, D.; Gaubicher, J.; Boucher, F. *Chem. Mater.* **2010**, *22*, 4126.
(18) Yuan, A. Q.; Wu, J.; Bai, L. J.; Ma, S. M.; Huang, Z. Y.; Tong, Z. F. *J. Chem. Eng. Data* **2008**, *53*, 1066.
(19) Basset, H.; Bedwell, W. *J. Chem. Soc.* **1933**, 854.
(20) Koleva, V. G. *Spectrochim. Acta, Part A* **2005**, *62*, 1196.
(21) Yuan, A. Q.; Wu, J.; Huang, Z. Y.; Wu, K.; Liao, S.; Tong, Z. E. *Mater. Res. Bull.* **2008**, *43*, 1339.
(22) Ellis, B.; Kan, W. H.; Makahnouk, W. R. M.; Nazar, L. F. *J. Mater. Chem.* **2007**, *17*, 3248.
(23) Bramnik, N. N.; Ehrenberg, H. *J. Alloys Compd.* **2008**, *464*, 259.
(24) Badi, S. P.; Ramesh, T. N.; Ellis, B.; Lee, K. T.; Nazar, L. F. Abstract 397, 216th ECS Meeting, Vienna Austria, 2009.
(25) Gardiner, G. R.; Islam, M. S. *Chem. Mater.* **2010**, *22*, 1242.
(26) Yamada, A.; Kudo, Y.; Liu, K. Y. *J. Electrochem. Soc.* **2001**, *148*, A1153.
(27) Malik, R.; Zhou, F.; Ceder, G. *Phys. Rev. B* **2009**, 79.
(28) Molenda, J.; Qjczyk, W.; Marzec, J. *J. Power Sources* **2007**, *174*, 689.
(29) Wagemaker, M.; Borghols, W. J. H.; Mulder, F. M. *J. Am. Chem. Soc.* **2007**, *129*, 4323.